Small Dual-Band 3D Beamforming MIMO Antenna

Abel Zandamela[#1], Nicola Marchetti[#2], and Adam Narbudowicz[#3]

[#]CONNECT Centre, Trinity College Dublin, The University of Dublin, Dublin 2, Ireland

{[1]zandamea, [2]nicola.marchetti, [3]narbudoa}@tcd.ie

Abstract — This work proposes a small dual-band (2.4 GHz and 4.89 GHz bands) 3D beamforming Multiple-Input Multiple-Output (MIMO) antenna for emerging size-constrained Internet of Things (IoT) applications. The performance is realized via digital beamforming in a structure sized only 51.5 mm in diameter (smaller than half wavelength at 2.4 GHz). At the 2.4 GHz band, the antenna realizes an isolation > 30 dB, and the Envelope Correlation Coefficient (ECC) is < 0.0003), with a bi-directional beamforming capability in the azimuth plane, and unidirectional beamforming across the elevation plane. At the 4.89 GHz band, the isolation is > 19 dB, and the ECC< 0.0047, while unidirectional beamforming is achieved in both the azimuth and elevation planes.

Keywords — Beamforming antennas, MIMO antennas, multi-band antennas, small pattern reconfigurable antennas.

I. INTRODUCTION

The IoT paradigm, as one of the most promising technological innovations in society at large, has become increasingly indispensable to many emerging smart wireless systems like, smart homes, smart cities, and healthcare systems [1], [2]. However, such applications place tight physical constraints on the total available space for antenna installation. Furthermore, many IoT applications [e.g., localization via Angle of Arrival (AoA) estimation, MIMO systems, emerging physical layer security techniques] require multiple antennas to achieve advanced beamforming characteristics [2], [3], [4].

In the state-of-the-art, classical antenna arrays are integrated into IoT devices. However, array elements need inter-spacing d (typically $\lambda/2$, where λ is the wavelength at the center operating frequency). This allows for mutual coupling mitigation; however, it also results in large space requirements, which limits their integration in size-constrained IoT devices (e.g., wrist and foot wearables). Different works have studied compact multi-band beamforming antennas, e.g., [5], [6], [7], [8]. The work in [5] proposes a center-shorted microstrip antenna for smart communication systems; the design is loaded with varactors to switch between omnidirectional and broadside patterns in different frequency bands. The study in [6] presents a stacked-patch antenna covering the Medical Body Area Network bands (2.31 GHz – 2.41 GHz) and the 5.8 GHz ISM band, with omnidirectional and broadside patterns. In [7], annular ring and Substrate Integrated Waveguide technology are used for the broadside and omnidirectional patterns in 5.8 GHz and 30 GHz bands. Lastly, coupled shorted patch antennas are employed for dual-band and beamforming in Narrow Band (NB)-IoT devices for on/off-body wireless communications in [8]. While the above works offer improvements in beamforming and multi-band properties, the achieved beamforming performance is limited to a few discrete states (omnidirectional or broadside patterns) [5], [6], [7], [8]; such performance is not sufficient for practical IoT applications like AoA estimation, as it is often desired to detect the signals incoming from different angles in the azimuth or elevation planes, therefore requiring continuous beamforming across different planes.

In this work, we propose for the first time a 9-port MIMO antenna capable of dual-band 3D beamforming. The structure comprises stacked-patch antennas and has a diameter of 51.5 mm (0.41λ at 2.4 GHz). The beamforming is realized by controlling the phase and amplitude of the antenna ports. Furthermore, it is demonstrated that at the lower-band bi-directional (azimuth) and unidirectional (elevation) patterns are realized with isolation > 30 dB and ECC< 0.0003. In the upper band, a unidirectional pattern is realized in both planes while providing isolation > 19 dB, and ECC< 0.0047.

II. BEAMFORMING AND MULTI-BAND PRINCIPLES

A. Beamforming Principle

The antenna beamforming characteristics are realized through the excitation of omnidirectional phase-varying spherical modes (SMs) [9]. SMs are true solutions of the vector wave equation and form an orthogonal basis on the sphere circumscribing the antenna [10]. They are often used in near-field spherical measurements for antenna pattern representation. To achieve beamforming in the azimuth plane, omnidirectional SMs of different order with their phase changing in two opposing directions (clockwise and counter-clockwise) are excited within the same antenna volume. By controlling the phase and amplitudes of each excited SM, unidirectional beamsteering covering the entire azimuth plane is realized (see [9] for a detailed discussion).

For beamforming in the elevation plane, broadside radiating modes are used. The modes are obtained as the dominant modes, e.g., for rectangular or circular microstrip antennas without any reactive loading. Since the broadside modes have the main beam pointing towards $\theta = 0°$, the SMs can be simultaneously excited to steer the main beam direction away from $\theta = 0°$ by controlling the phase and amplitudes of the antenna ports. Note that the scanning range in the elevation plane can be changed by increasing the number of simultaneously excited SMs.

B. Multi-Band Principle

The proposed multi-band operation is depicted in Fig. 1. The principle is based on the excitation of SMs of the same
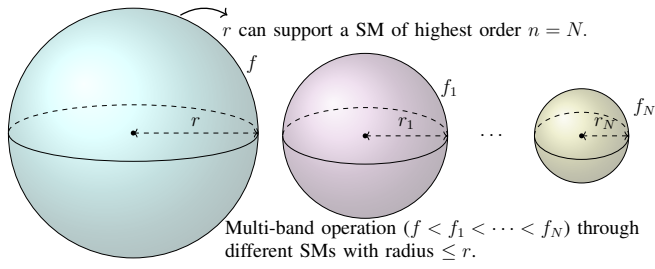
Fig. 1. Schematic of the proposed multi-band operation principle. The method is based on the excitation of different SMs required for beamforming but at higher frequency bands.

order at higher frequency bands. Assuming that within r (the smallest radius of a sphere that can fully enclose the antenna), the highest phase-varying SM is realized at frequency f, the same mode can then be excited at higher frequencies $f < f_1 < f_2 < \cdots < f_N$ using radius $r > r_1 > r_2 \cdots > r_N$. Several advantages can be achieved using the proposed concept, e.g.:

- The overall diameter of the device is unchanged, i.e., the excited SMs for multi-band operation have radius $\leq r$.
- By using collocated and concentric ring structures, different-order SMs at multiple bands can be excited using different antenna layers, which allows full use of the volume of the sphere circumscribing the antenna.
- Good isolation is achieved as SMs are orthogonal, and the same order SM with the same phase variations are only excited at different frequency bands.
- 3D beamforming principle is unchanged as the difference is in the frequency of operation.

It is worth mentioning that the challenge of the proposed principle is mainly related to the design of a practical feeding system to excite all the SMs required for beamforming at different frequency bands.

III. ANTENNA DESIGN

Fig. 2 shows the antenna proposed to realize the beamforming and multi-band methods discussed in Section II. It comprises four-stacked layers (see Fig. 2a) separated by three Styrofoam layers ($\epsilon_r = 1$ and $0.5\,\mathrm{mm}$ thickness), and supports dual-band operation: $f_1 = 2.4\,\mathrm{GHz}$ and $f_2 = 4.89\,\mathrm{GHz}$. The top-layer (L1) shown in Fig. 2b comprises a patch exciting two TM_{21} modes to provide dual-phase variations in the xy-plane at f_2. The patch is supported by a $1.27\,\mathrm{mm}$ thick TMM6 substrate ($\epsilon_r = 6.3$, $\tan\delta = 0.0023$). Its diameter is $D_1 = 24.8\,\mathrm{mm}$, and the feeding positions are P(x, y): P5 ($5\,\mathrm{mm}, 0\,\mathrm{mm}$) and P6 ($3.5\,\mathrm{mm}, 3.5\,\mathrm{mm}$).

Fig. 2c shows layer-3 (L3), supported by a $1.27\,\mathrm{mm}$ TMM10 substrate ($\epsilon_r = 9.8$, $\tan\delta = 0.0022$), and includes a shorted-pin central patch and an annular ring patch. The central patch (diameter $D_2 = 11.8\,\mathrm{mm}$) is center-fed using P7, and includes 8 vias of $0.5\,\mathrm{mm}$ diameter, which are rotated by $45°$ and located $4\,\mathrm{mm}$ away from the center. This configuration excites a monopole-like pattern providing a constant phase around xy−plane at f_2. The annular ring structure (outer
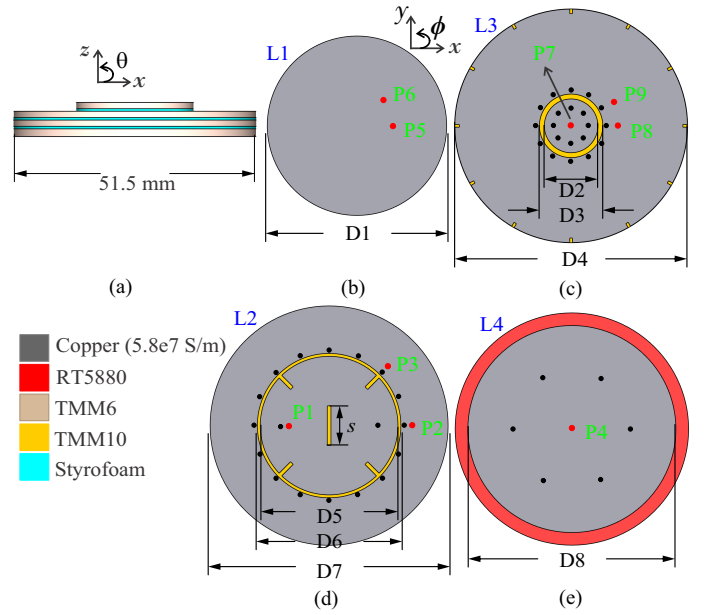

Fig. 2. Proposed antenna to realize the beamforming and multi-band methods discussed in Section II: (a) front view highlighting device diameter and thickness; (b) exploded view showing different substrate layers and ports arrangement for each layer.

diameter $D_4 = 51.5\,\mathrm{mm}$) is shorted using 12 vias and 12 slits rotated by $30°$. The vias are located $1\,\mathrm{mm}$ from the edges of the inner diameter ($D_3 = 14\,\mathrm{mm}$), while the slits have width $0.6\,\mathrm{mm}$, and length $0.8\,\mathrm{mm}$. The annular ring is fed using P8 ($9.2\,\mathrm{mm}, 0\,\mathrm{mm}$) and P9 ($8\,\mathrm{mm}, 4.5\,\mathrm{mm}$), exciting TM_{31} modes with triple-phase variations around the azimuth plane also at f_2.

Fig. 2d shows L2, which integrates a central patch and an annular ring. The layer uses a $1.27\,\mathrm{mm}$ thick TMM10 substrate. The centrally located patch has a diameter $D_5 = 29.8\,\mathrm{mm}$. It includes two vias located at ($-10.5\,\mathrm{mm}, 0\,\mathrm{mm}$) and ($10.5\,\mathrm{mm}, 0\,\mathrm{mm}$), and a central slot of length $s = 8.5\,\mathrm{mm}$, width $0.8\,\mathrm{mm}$. Four additional slots of length $3.6\,\mathrm{mm}$ and width $0.8\,\mathrm{mm}$ are integrated for frequency tuning, and P1 ($-9\,\mathrm{mm}, 0\,\mathrm{mm}$) is used to excite a broadside radiating mode at f_1 and f_2. The second component of L2 - annular ring (outer diameter $D_7 = 51.5\,\mathrm{mm}$) - is shorted using 16 vias rotated by $22.5°$ and located $1\,\mathrm{mm}$ from the edges of the inner diameter ($D_6 = 31\,\mathrm{mm}$). The ring is fed using P2 ($18\,\mathrm{mm}, 0\,\mathrm{mm}$), P3 ($12.5\,\mathrm{mm}, 12.5\,\mathrm{mm}$) and excites two TM_{21} modes at f_1.

Lastly, the bottom layer (L4) shown in Fig. 2e is supported by a $1.57\,\mathrm{mm}$ thick RT5880 substrate ($\epsilon_r = 2.2$, $\tan\delta = 0.0009$). The layer includes a center-fed (P4) shorted-pin patch antenna of diameter ($D_4 = 45.8\,\mathrm{mm}$), shorted with 6 vias rotated by $60°$ and located $13\,\mathrm{mm}$ away from the center, to excite an xy-plane constant phase monopole-like pattern at f_1.

The total thickness of the device is $7.15\,\mathrm{mm}$ and the diameter is $51.5\,\mathrm{mm}$, in terms of wavelength (at $2.4\,\mathrm{GHz}$) the size is: $0.41\lambda \times 0.41\lambda \times 0.057\lambda$, providing a miniaturized and low-profile antenna for space-constrained IoT applications.
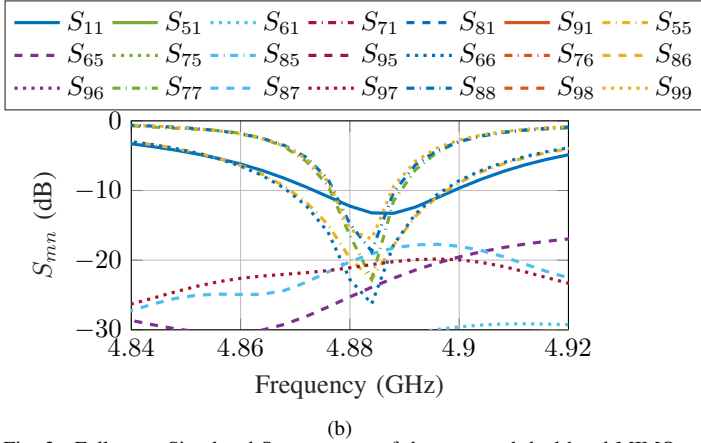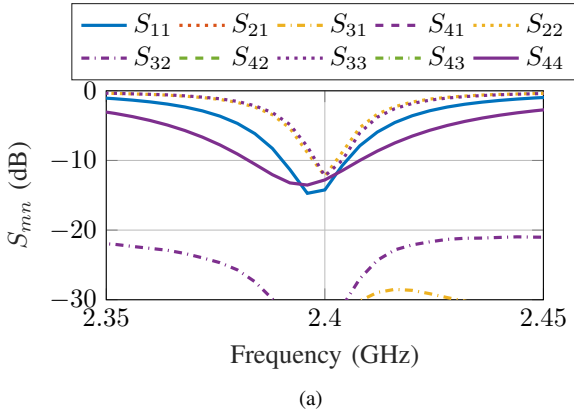
(a)

(b)

Fig. 3. Full-wave Simulated S-parameters of the proposed dual-band MIMO antenna: (a) $f_1 = 2.4\,\text{GHz}$ band and (b) $f_2 = 4.89\,\text{GHz}$ band.

(a)

(b)

Fig. 4. Color-coded ECC values of the proposed MIMO antenna: (a) $f_1 = 2.4\,\text{GHz}$, and (b) $f_2 = 4.89\,\text{GHz}$.

IV. SIMULATED RESULTS

The antenna is simulated using a 3D finite element method full-wave solver. The S-parameters are shown in Fig. 3. The isolation between all the ports is better than $30\,\text{dB}$ in $f_1 = 2.4\,\text{GHz}$ (Fig. 3a) and $19\,\text{dB}$ in $f_2 = 4.89\,\text{GHz}$ (Fig. 3b). The ECC is evaluated using the complex 3D radiation patterns of each port of the proposed MIMO antenna

$$\rho_{ECC} = \frac{\left|\iint_{4\pi}[F_m(\theta,\phi) \cdot F_n(\theta,\phi)]d\Omega\right|^2}{\iint_{4\pi}|F_m(\theta,\phi)|^2 d\Omega \iint_{4\pi}|F_n(\theta,\phi)|^2 d\Omega} \quad (1)$$

where m and n represent different antenna ports in a given band. The ECC values for f_1 are below 0.0003 (see Fig. 4a), and for f_2 are below 0.0047 (see Fig. 4b).

The beamforming performance is shown in Fig. 5 for f_1 and f_2. Because the monopole-like patterns (P4 and P7) have a constant phase in the azimuth plane, these ports are used as the reference port. Assuming that at a desired direction ϕ_{dir} the phase of the radiation pattern of a phase varying mode is $Phase_{Pn}$, the required phase shift to steer the beam to ϕ_{dir} is computed using

$$\Delta P_n = Phase_{P_{reference}} - Phase_{Pn} \quad (2)$$

The computed phase shifts using (2) for azimuth plane beamsteering in f_1 are shown in Table 1. Fig. 5a shows the
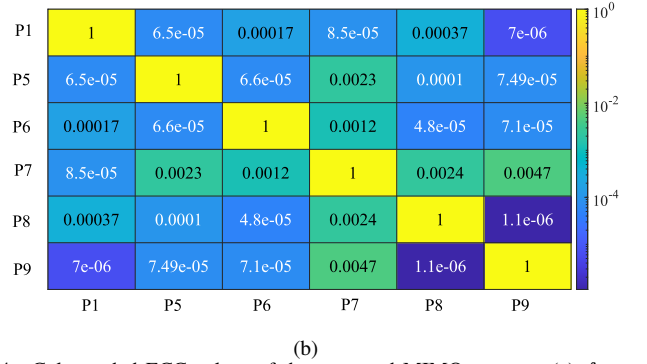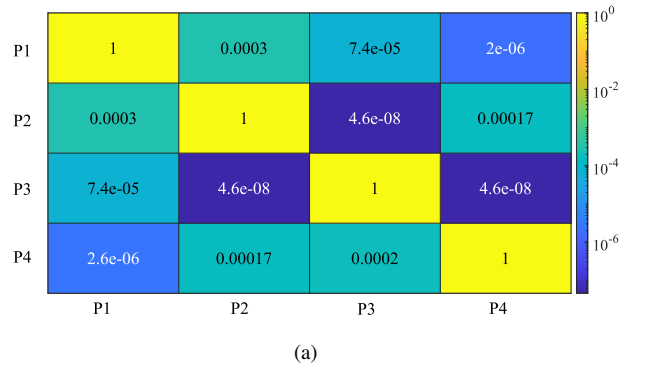
beamsteering performance around the azimuth plane for f_1 at two different directions, i.e. $\phi_{dir} = 0°$ and $90°$. Note that for this band, a second main beam is also observed at $\phi_{dir}+180°$. This ambiguity occurs because only the modes with dual-phase variations (P2 and P3) are used for beamforming in the f_1 band. To eliminate this ambiguity, higher-order modes can be integrated to improve the directivity of the device. This is shown in Fig. 5c, where the modes with triple phase variations are also used (P8 and P9) for f_2 band beamforming, hence providing a unidirectional pattern. The azimuth plane beamforming in f_2 (Fig. 5c) is shown for four different directions separated by $90°$ to cover the entire azimuth plane, and the phase shifts values are also computed using (2) and are shown in Table 1.

The beamforming in the elevation plane for f_1 frequency band is shown in Fig. 5b. It is obtained by combining the broadside radiating mode (excited using P1) and one of the two phase-varying modes (P2/P3). For brevity, only the $yz-$plane performance is discussed. It is seen that the main beam direction can be steered away from the broadside $\theta = 0°$ towards $\theta = 20°$ and $-20°$; the corresponding phase shifts for each excited port are reported in Table 1. Fig. 5d shows the performance for the elevation plane in f_2 band, around the $yz-$plane. The results are obtained using all the modes required for beamforming in the azimuth plane while simultaneously activating the broadside radiating mode (excited using port P1). Note that this offers a wider steering range when compared to the performance shown for the f_1
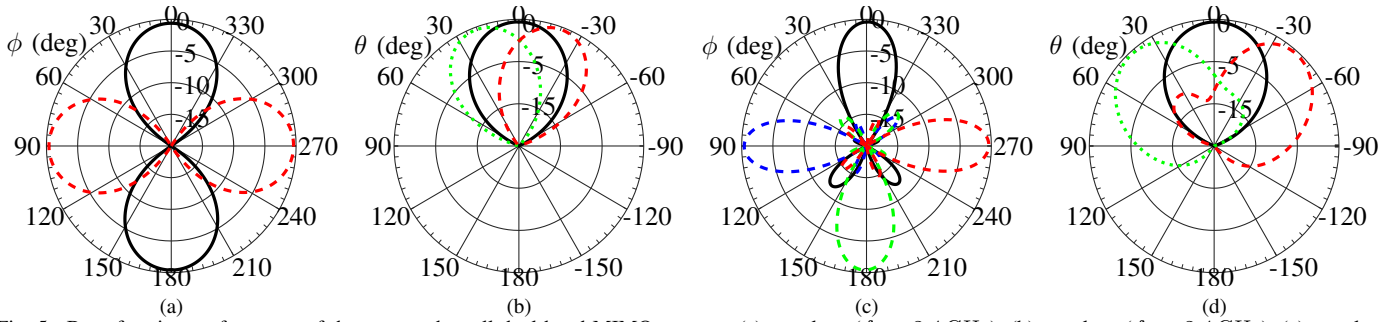
Fig. 5. Beamforming performance of the proposed small dual-band MIMO antenna: (a) xy-plane ($f_1 = 2.4\,\text{GHz}$); (b) yz-plane ($f_1 = 2.4\,\text{GHz}$); (c) xy-plane ($f_2 = 4.89\,\text{GHz}$); and (d) xz-plane ($f_2 = 4.89\,\text{GHz}$). The respective port configurations for each direction are shown in Table 1.

Table 1. Phase Configurations (ΔP_n) of each antenna port for beamforming in f_1 and f_2 bands, all ports are excited with similar input amplitudes.

Freq.		Beamforming Direction	ΔP1	ΔP2	ΔP3	ΔP4	ΔP5	ΔP6	ΔP7	ΔP8	ΔP9
$f_1 = 2.4\,\text{GHz}$	xy-plane	$\theta = 90°, \phi = 0°/180°$	-	$-14°$	$76°$	$0°$	-	-	-	-	-
		$\theta = 90°, \phi = 90°/270°$	-	$164°$	$253°$	$0°$	-	-	-	-	-
	yz-plane	$\theta = 0°, \phi = 90°$	$0°$	-	-	-	-	-	-	-	-
		$\theta = 21°, \phi = 90°$	$160°$	$30°$	-	-	-	-	-	-	-
		$\theta = -21°, \phi = 90°$	$0°$	-	$-30°$	-	-	-	-	-	-
$f_2 = 4.89\,\text{GHz}$	xy-plane	$\theta = 90°, \phi = 0°$	-	-	-	-	$84°$	$-2°$	$0°$	$170°$	$83°$
		$\theta = 90°, \phi = 90°$	-	-	-	-	$-87°$	$178°$	$0°$	$-98°$	$-5°$
		$\theta = 90°, \phi = 180°$	-	-	-	-	$94°$	$11°$	$0°$	$-9°$	$-96°$
		$\theta = 90°, \phi = 270°$	-	-	-	-	$-94°$	$167°$	$0°$	$85°$	$173°$
	xz-plane	$\theta = 0°, \phi = 0°$	$0°$	-	-	-	-	-	-	-	-
		$\theta = 42°, \phi = 0°$	$0°$	-	-	-	$84°$	$-2°$	$0°$	$170°$	$83°$
		$\theta = -45°, \phi = 0°$	$-30°$	-	-	-	$94°$	$11°$	$0°$	$-9°$	$-96°$

frequency band (Fig. 5b). This is explained by the use of an increased number of phase-varying spherical modes in the f_2 band.

V. CONCLUSIONS

This work proposed a compact MIMO antenna for 3D beamforming in two different frequency bands ($2.4\,\text{GHz}$ and $4.89\,\text{GHz}$). The beamforming and multi-band principles are validated through full-wave simulations, highlighting that the antenna achieves isolation better than $19\,\text{dB}$ and ECC< 0.0047 across the two bands. Because of its compact diameter and low profile, the antenna is proposed to enable advanced wireless radio applications in emerging size-constrained IoT applications.

ACKNOWLEDGMENT

REFERENCES

[1] Y. A. Qadri, A. Nauman, Y. B. Zikria, A. V. Vasilakos, and S. W. Kim, "The Future of Healthcare Internet of Things: A Survey of Emerging Technologies," *IEEE Commun. Surveys Tuts.*, vol. 22, no. 2, pp. 1121–1167, 2020.

[2] H. Obeidat, W. Shuaieb, O. Obeidat, and R. A. Abd-Alhameed, "A Review of Indoor Localization Techniques and Wireless Technologies," *Wirel. Personal Commun.*, vol. 119, pp. 289 – 327, 2021.

[3] Y. Ding and V. Fusco, "Directional-modulation-enabled physical-layer wireless security," in *Trusted Communications with Physical Layer Security for 5G and Beyond*. Institution of Engineering and Technology, 2017, ch. 13, pp. 313–336.

[4] A. Zandamela, A. Chiumento, N. Marchetti, and A. Narbudowicz, "Angle of Arrival Estimation via Small IoT Devices: Miniaturized Arrays vs. MIMO Antennas," *IEEE Internet Things Mag.*, vol. 5, no. 2, pp. 146–152, 2022.

[5] N. Nguyen-Trong, L. Hall, and C. Fumeaux, "A Frequency- and Pattern-Reconfigurable Center-Shorted Microstrip Antenna," *IEEE Antennas Wireless Propag. Lett.*, vol. 15, pp. 1955–1958, 2016.

[6] X.-Q. Zhu, Y.-X. Guo, and W. Wu, "Miniaturized Dual-Band and Dual-Polarized Antenna for MBAN Applications," *IEEE Trans. Antennas. Propag.*, vol. 64, no. 7, pp. 2805–2814, 2016.

[7] B. J. Xiang, S. Y. Zheng, H. Wong, Y. M. Pan, K. X. Wang, and M. H. Xia, "A Flexible Dual-Band Antenna With Large Frequency Ratio and Different Radiation Properties Over the Two Bands," *IEEE Trans. Antennas. Propag.*, vol. 66, no. 2, pp. 657–667, 2018.

[8] Z. Shao and Y. Zhang, "Design and Modeling of Dual-Band Dual-Mode Coupled Shorted Patch Antennas," *IEEE Trans. Antennas. Propag.*, vol. 69, no. 12, pp. 8237–8247, 2021.

[9] A. Zandamela, N. Marchetti, M. J. Ammann, and A. Narbudowicz, "Spherical Modes Driven Directional Modulation with a Compact MIMO Antenna," *IEEE Antennas Wirel. Propag. Let.*, vol. 22, no. 3, pp. 1–5, 2022.

[10] J. E. Hansen, Ed., *Spherical Near-field Antenna Measurements*, ser. Electromagnetic Waves. Institution of Engineering and Technology, 1988.